



Assessment of force control for surface finishing – an experimental comparison between Universal Robots UR10e and FerRobotics active contact flange

Stefan Gadringer, Hubert Gattringer, and Andreas Mueller

Institute of Robotics, Johannes Kepler University Linz, Altenbergerstr. 69, 4040 Linz, Austria

Correspondence: Stefan Gadringer (stefan.gadringer@jku.at)

Received: 15 December 2021 – Revised: 23 February 2022 – Accepted: 10 March 2022 – Published: 21 April 2022

Abstract. Robotic surface treatment is already broadly used in the manufacturing industry because it guarantees repeatable high-quality surfaces at short production time. Such a robotic solution, with an accurate control of the applied force on a surface, requires a robot that is either equipped with a force/torque sensor or, alternatively, with a force compliance device. However, without a direct performance comparison, it is hard to know which is the best option for a specific surface treatment operation. Compared to the evaluation of the robot positioning accuracy, using the ISO 9283 test, no standardized test for the quality assessment of robot force control exists yet. In trying to fill this gap, this paper introduces different test scenarios and a test set-up for such a force control quality assessment. As a start, the force control of a Universal Robots UR10e model and a FerRobotics ACF-K 109/04 model are experimentally evaluated. The latter is an external device with controlled force/compliance characteristics, which is referred to as an active contact flange (ACF). For the performance comparison, an ATI force/torque sensor, which is mounted below a work piece, measures the applied force either by the UR or by the ACF. The measured forces are further transformed to the UR tool centre point (TCP) frame. Then, only the z component of the force, or rather the normal force, is relevant for surface treatment and hence important for the evaluation. For each test case, the average value of five test runs with the same parameters is used for the assessment. Results for both the UR and ACF force control are presented for varying desired contact velocities and desired forces. These results indicate the advantage of the ACF-K 109/04 over the UR10e force control for highly dynamic force control scenarios.

1 Introduction

Surface finishing operations like grinding, sanding, or polishing are common in many industrial sectors, for example, in the automotive industry or aerospace (Iglesias et al., 2015). Previously, such operations were mainly carried out by people. These days, industrial robots are used more and more for the reduction of labour and further increase in the efficiency and quality. Force-controlled robots are even used for machining operations. Active force control is limited by the control bandwidth, which limits its use to applications with low dynamics. On the other hand, devices that actively control the passive compliance allow for the generation of a prescribed passive (physical) compliance. They represent alternatives to force-controlled robots using force/torque sensors. There are

a number of commercial, so-called compliance devices, that can be used for surface treatment, such as the FerRobotics active contact flange (ACF; FerRobotics Compliant Robot Technology GmbH, 2021a), ATI PCFC (ATI Industrial Automation, 2021b), the Robotiq sanding kit, or the force compliance devices of PushCorp (PushCorp Inc., 2021).

Passive compliance tools (with open-loop control) set the desired force via external, manually adjusted air pressure regulators. The force for a specific pressure is constant, provided that the tool inclination stays the same for the whole operation. In contrast, active compliance devices rely on internal closed-loop feedback control to actively control the compliance, and to compensate for gravity, independent of the tool orientation.

From an application perspective, in order to decide whether the active compliance provided by an industrial robot is sufficient, or if controlled compliance devices are necessary, it is crucial to perform representative tests for comparative performance assessments. For example, Winkler and Suchý (2013) use a triangular contour to assess the quality of the hybrid position/force controller of a robot. However, there is neither a standardized test nor are there standardized performance measures. In this paper, a testing procedure and assessment criteria that allow for an objective comparison are proposed. The test regime is applied to the UR10e (Universal Robots A/S, 2021) and the ACF-K 109/04 (FerRobotics Compliant Robot Technology GmbH, 2021b), which is an active compliance tool. A detailed explanation of the test scenarios, the test set-up, including computer-aided design (CAD) data, and all results are publicly available on the GitHub repository of JKU Linz – Institute of Robotics. This enables the reproduction of the results for the presented two systems but also to perform these tests for other systems.

2 Desired characteristics

Figure 1 visualizes the desired characteristics of a robotic surface finishing system. Thus, robots with or without force compliance tools should do the following:

1. have a high performance,
2. exhibit a high robustness,
3. be simple to programme, and
4. show flexibility.

First, a high performance is desired. In the context of surface treatment, this means a high accuracy of normal forces, together with a short settling time and short transient oscillation, to be able to achieve high-quality surfaces. A high finishing speed assures short cycle times.

Second, both the robot and the tool should have high robustness to endure possible high, normal, and shear forces. High forces could occur during normal operation (e.g. grinding and deburring) or during a collision, in the worst-case scenario.

Third, the programming complexity for following a desired path of the tool centre point (TCP), which depends on the used robotic set-up (robot and tool), should be low. Using a force compliance tool for surface treatment might simplify the planning of the TCP trajectory because the robot just needs to operate in position control mode. In this case, the tool is responsible for applying the desired normal force while compensating for position deviations of the robot. By contrast, without the force compliance tool, the robot must operate in force control mode, and task-dependent controller settings are required for appropriate control of the normal force while following the TCP path.

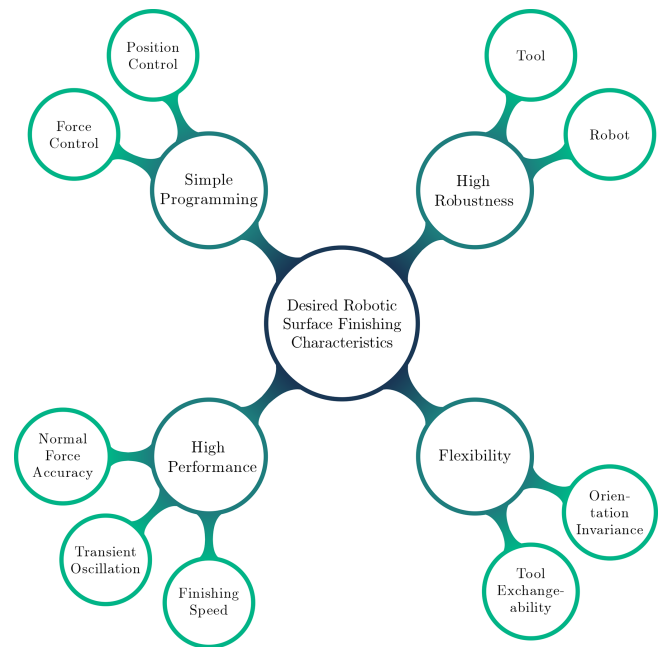


Figure 1. Desired robotic surface finishing characteristics.

The fourth desired characteristic is flexibility, which mainly implies orientation invariance and tool exchangeability. If the former criterion is fulfilled, then a desired force can be applied independently of the tool inclination. So, a different end effector orientation due to a changed robot trajectory or an inclined tool mounting position would have no negative effect. The latter criterion describes if or how easily a robot tool can be exchanged to replace a broken hardware or be ready for another task such as, for example, switching from grinding to polishing.

3 Control of active and passive compliance

For machining operations via robots, a safe contact or rather a compliant behaviour between the robot and its environment must be ensured. For example, the control of the active compliance is possible via impedance control (Siciliano and Villani, 1999), which is shown in Fig. 2.

The apparent compliance is achieved by a controlled evasive motion as a response to the measured forces. This is obtained within the control cycle time. The impedance controller uses the desired trajectory, the measured joint position \mathbf{q} and velocity $\dot{\mathbf{q}}$, and the measured contact forces and torques at the end effector $\mathbf{h}_e \in \mathbb{R}^6$ as input. Thereby, the desired trajectory is given by the corresponding position $\mathbf{r}_d \in \mathbb{R}^3$, orientation $\mathbf{R}_d \in \text{SO}(3)$, and their derivatives up to translational acceleration $\ddot{\mathbf{r}}_d \in \mathbb{R}^3$ and angular acceleration $\dot{\boldsymbol{\omega}}_d \in \mathbb{R}^3$. As described in Siciliano and Villani (1999), the output of the impedance controller $\boldsymbol{\alpha} \in \mathbb{R}^6$ is computed, so that together with the inverse dynamics control law, the robot behaviour is equivalent to a mass–spring–damper sys-

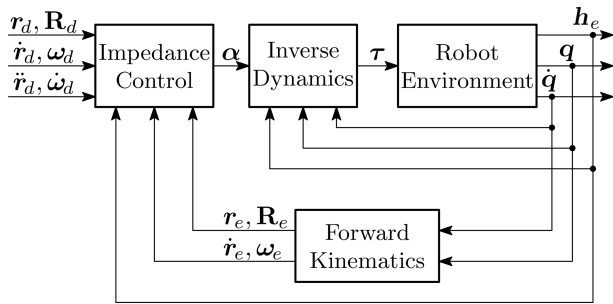


Figure 2. Block diagram of impedance control (adapted from Siciliano and Villani, 1999).

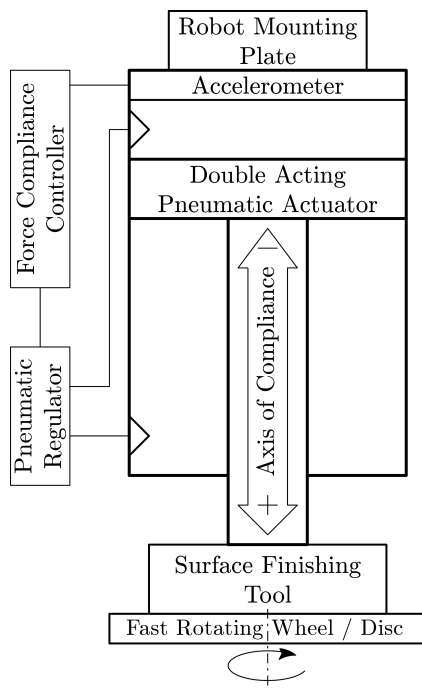


Figure 3. Working principle of an active force compliance device.

tem. Due to the required inverse dynamics, impedance control is a model-based control scheme and requires an accurate dynamic model of the robot (Bremer, 2008).

On the other hand, active compliance devices actively control the passive compliance. Using such a device decouples the robot from the contact process and hence from contact forces at the end effector, occurring during surface finishing operations for example. Such a decoupling simplifies robot control to just position control due to the independence from the environment.

Figure 3 shows the working principle of an active force compliance device. Such a device can basically be a double-acting pneumatic actuator with additional sensors. A surface finishing tool is somehow attached to the cylinder piston, which represents the axis of compliance. The force compliance controller continuously adjusts the pressure via the

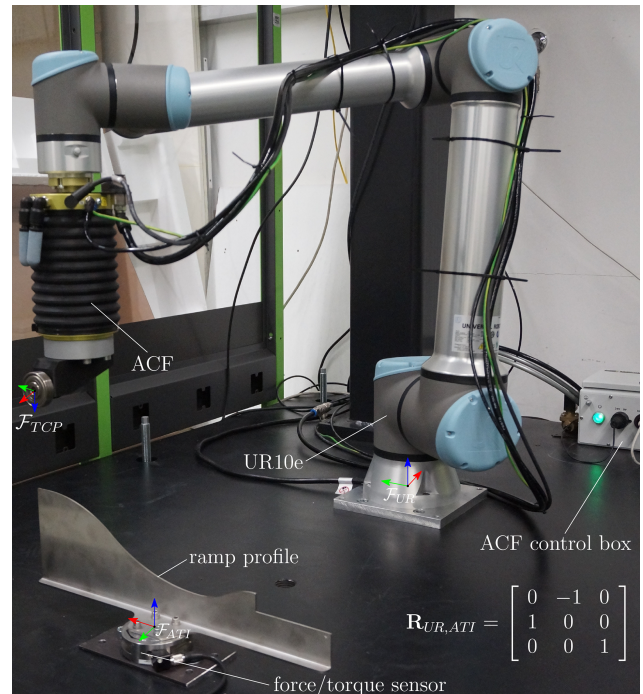


Figure 4. Measurement set-up with UR10e, ACF, and the force/torque sensor.

pneumatic regulator (closed loop) to apply the desired force while compensating for gravity using the accelerometer measurement. Some manufacturers, e.g. PushCorp Inc. (2021), additionally attach a load cell to the double-acting pneumatic actuator to directly read the force applied by the actuator. In contrast, FerRobotics Compliant Robot Technology GmbH (2021a) accurately calibrates each ACF for different orientations before product delivery to be able to apply the desired force independently from the orientation.

4 Test set-up

Figure 4 shows the test set-up with Universal Robots UR10e, a robot tool, and a force/torque sensor as the main components. Different profiles (e.g. ramp profile) allow for the comparison of the UR/ACF force control for various test cases. The force/torque sensor is mounted at the bottom of a work piece for measuring the real forces acting on the work piece. The robot tool itself consists of the ACF, an iron reel, and an additional adjustable weight for the simulation of a real robot tool (e.g. angle grinder), which would normally be mounted on the ACF-K (FerRobotics Compliant Robot Technology GmbH, 2021b) instead of the reel. The ACF requires a separate control box for operation.

The ATI Delta SI-660-60 (ATI Industrial Automation, 2021a) of Fig. 4 serves as force/torque sensor for the assessment. It has a sensing range up to 1980 N and a resolution of 0.25 N for normal forces, i.e. forces F_z . The ATI forces

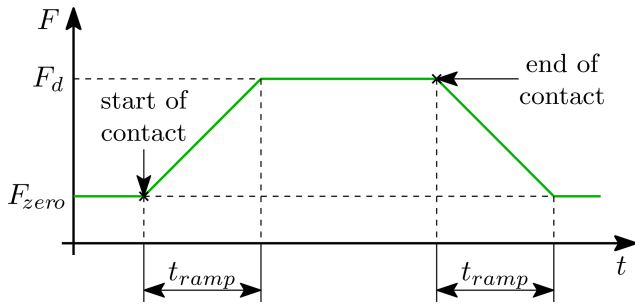


Figure 5. Force evolution depending on ACF operation parameters (adapted from FerRobotics Compliant Robot Technology GmbH, 2021c).

are read with a sample time of 800 μs using a B&R analogue input module of the B&R X20 CPU (B&R Industrial Automation GmbH, 2021a, b).

4.1 Universal Robots

The Universal Robots UR10e model (Universal Robots A/S, 2021) is a collaborative robot with 6 degrees of freedom (DOF). It allows a maximal payload of 10 kg and has a built-in force/torque sensor. According to the specification, the UR10e has a control frequency of 500 Hz (2 ms sampling time) and allows force control up to 100 N, with an accuracy of 5.5 N.

Surface finishing requires the control of the normal force. Hence, for the UR force control, it is necessary to set the z axis of the TCP frame \mathcal{F}_{TCP} as the compliant axis. This means that the force control task frame must be equal the current TCP frame. Consequently, the task frame must be continuously updated to guarantee this even during movement. The UR further allows the modification of the force control via the parameters of damping $0 \leq d \leq 1$ (default 0.005) and gain scaling $0 \leq \text{gain} \leq 2$ (default 1). The damping parameter describes the UR speed decrease behaviour in the case of no contact with a work piece. In detail, using a damping parameter greater than zero leads to a deceleration if no force is present. The gain scaling parameter represents the gain of the force controller. A larger value than the default value of 1 leads to a more aggressive controller and might even cause instability.

4.2 Active contact flange

In contrast to the UR, the ACF is a 1 DOF mechatronic actuator and sensor element. This enables a robot with a mounted ACF to apply a consistent contact force on a surface, even if it is not equipped with a force/torque sensor. The product to be tested is an ACF-K 109/04, with a stroke of 35.5 mm and a maximal applicable force of 100 N (FerRobotics Compliant Robot Technology GmbH, 2021b).

Figure 5 shows an exemplary ACF force evolution for a desired force $F_d \geq 0$, considering its operation parameters. The operation parameters are the ramp time $t_{\text{ramp}} \geq 0$ and zero force $0 \leq F_{\text{zero}} \leq F_d$, which describe a ramp used for ramping up from force F_{zero} to F_d within time t_{ramp} . Without contact to a work piece, the ACF initially applies a force of F_{zero} . As soon as contact is detected, the ACF ramps up to force F_d within the defined time. If t_{ramp} is zero, then the ramp is deactivated, and the ACF always applies F_d .

5 Test scenarios

This paper assesses three test scenarios (ramp profile, direct sensor contact, and straight profile) for the UR/ACF force control comparison. Due to the hard contact of the reel with a metal profile (metal-to-metal contact), quite high forces can result. The considered force control parameters are gain scaling gain = 1 and damping $d = 0$ for the UR and $t_{\text{ramp}} = 0$ s (deactivated force ramp) for the ACF. Tests with many more parameter values are presented on the GitHub repository of JKU Linz – Institute of Robotics (2022).

5.1 Ramp profile

The ramp profile of Fig. 6 involves various orientation changes and a ramp (or rather a jump) that will lead to a takeoff of the robot end-effector. Due to these fast orientation changes, highly dynamic force control is required for suitable performance. The TCP velocity is limited to 0.25 m s^{-1} .

5.2 Direct sensor contact

The direct sensor contact test, shown in Fig. 7, is simply a vertical movement directly onto the force/torque sensor of Fig. 6a, using an end-effector velocity of 0.10 or 0.25 m s^{-1} . Downwards, either the UR position or force control is used until the robot reaches the contact pose p_c , where it stands still for approx. 6 s and applies the desired force. Upwards, the UR uses position control for all test cases. This test considers the maximum ACF/UR force of 100 N to evaluate how well the ACF and the UR can handle such a high force.

5.3 Straight profile

Figure 8 shows the so-called straight profile, which is basically an aluminium profile, and it allows a movement speed up to 0.90 m s^{-1} due to its simple, straight shape. The length of the straight line is 0.53 m, which is approx. the total arc length of the ramp profile, to achieve a travel time like the other test case.

6 Assessment criteria

The assessment criteria are the deviation from the desired normal force, which should be applied to the work piece and

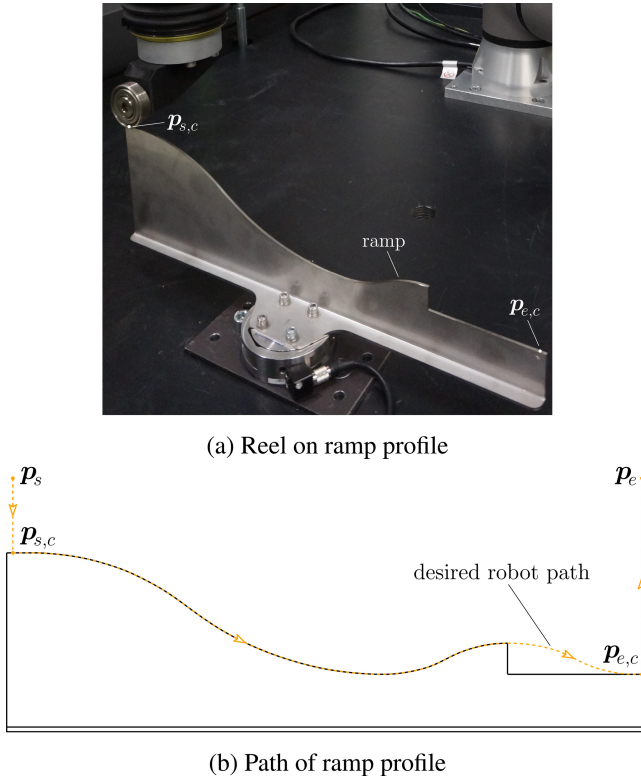


Figure 6. Robot path planning for the ramp profile.

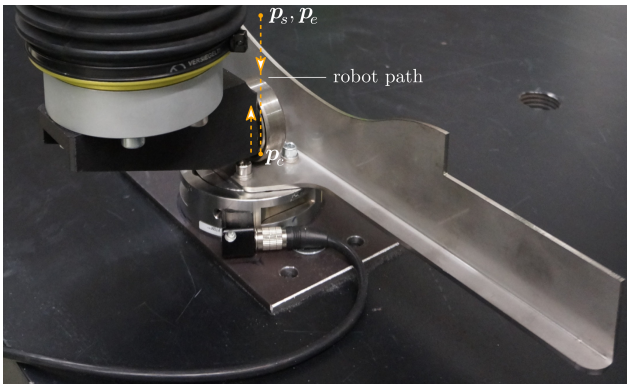


Figure 7. Robot path planning for the direct sensor contact.

the settling time to define the duration until the force error stays within a specified error band. If we consider a normal robot path to the surface of a work piece, then the normal force is equal the force F_z of the total force vector ${}_{\text{TCP}}\mathbf{F} = (F_x, F_y, F_z)^T$, represented in the TCP frame \mathcal{F}_{TCP} . However, the ATI force/torque sensor, shown in Fig. 4, measures the forces ${}_{\text{ATI}}\mathbf{F}$ in its own frame \mathcal{F}_{ATI} , and sampled with $800\ \mu\text{s}$, and further requires transformation to \mathcal{F}_{TCP} .

At first, the force vector is transformed to the UR base frame \mathcal{F}_{UR} , i.e. ${}_{\text{UR}}\mathbf{F} = \mathbf{R}_{\text{UR,ATI}} {}_{\text{ATI}}\mathbf{F}$, and subsequently to \mathcal{F}_{TCP} , i.e. ${}_{\text{TCP}}\mathbf{F} = \mathbf{R}_{\text{TCP,UR}} {}_{\text{UR}}\mathbf{F}$, using the actual TCP ori-

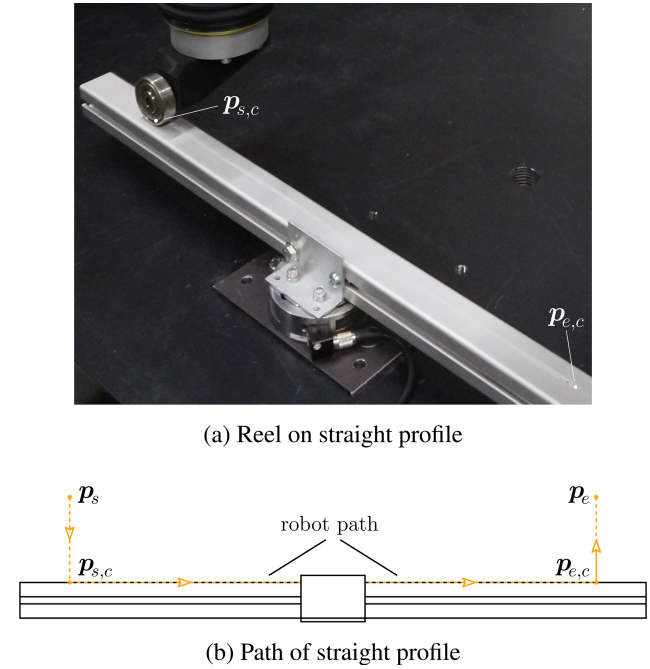


Figure 8. Robot path planning for the straight profile.

entation. This orientation is represented by the rotation matrix $\mathbf{R}_{\text{TCP,UR}}(\mathbf{q}) \in \text{SO}(3)$ and depends on joint coordinates $\mathbf{q} \in \mathbb{R}^6$. Therefore, the TCP orientation data must be sampled with $800\ \mu\text{s}$ as well. However, the UR10e internally uses a sampling time of $2\ \text{ms}$, i.e. upsampling is required. PolyScope 5.9.1, the UR operating system, represents the TCP orientation as a rotation vector, which is a compact form of the axis-angle representation (Siciliano and Khatib, 2016). For simplified data upsampling, this representation can also be converted to roll-pitch-yaw angles (Siciliano and Khatib, 2016), which is a consecutive rotation order of z - y - x , with angles γ - β - α , without a singularity problem because the robot mainly rotates about the x axis with the roll angle α . Considering these angles, data upsampling from $2\ \text{ms}$ to $800\ \mu\text{s}$ is easily possible, for example, via piecewise cubic interpolation (Fritsch and Carlson, 1980). Consequently, it is feasible to transform the ATI forces to \mathcal{F}_{TCP} and to calculate the absolute z -force error as follows:

$$\Delta F = F_d - F_z \quad \text{and} \quad \Delta \mathbf{F} = \mathbf{F}_d - \mathbf{F}_z. \quad (1)$$

Respectively, this is valid for a single measurement value or for the whole force path. This can be further separated into the two time domains, as follows:

$$\Delta \mathbf{F}_c = \Delta \mathbf{F} \Big|_{0 \leq t \leq t_c} \quad \text{and} \quad \Delta \mathbf{F}_p = \Delta \mathbf{F} \Big|_{t_m \leq t \leq t_e}. \quad (2)$$

The former represents the first few seconds of the standstill at the beginning (start of contact at $t = 0$) and is set to $t_c = 3\ \text{s}$ for both the ramp and the straight profiles and to $t_c = 6\ \text{s}$ for the direct sensor test. The latter considers the time

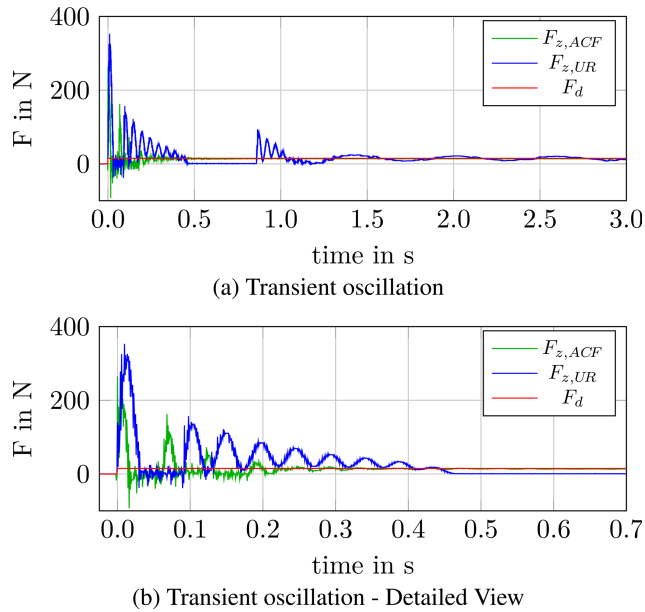


Figure 9. Force comparison at first contact for the ramp profile ($v_d = 0.25 \text{ m s}^{-1}$, $F_d = 15 \text{ N}$).

between the start of movement $t_m \geq t_c$ and the end time t_e . These times are determined automatically, using the desired velocity of the robot path. For the evaluation, the maximum absolute force error $\text{Max}|\Delta F|$ and the mean absolute error $\text{Mean}|\Delta F|$ with the corresponding standard deviation $\sigma|\Delta F|$ of both time domains are important.

In addition to the force error, the settling time t_{set} is another important criterion for the force control assessment. It defines the duration until the error stays within the error band of $\pm 10 \text{ N}$ or rather $\pm 10 \%$ of the maximal force of ACF and UR. For each test case, the average of five test runs with same parameters is used for the assessment.

7 Results

7.1 Ramp profile

Figure 9 shows the normal forces of ACF and UR10e at first contact with the ramp profile for a desired velocity of $v_d = 0.25 \text{ m s}^{-1}$ and a desired force of $F_d = 15 \text{ N}$. It can be seen in the detailed view of Fig. 9b that the ACF exhibits a much shorter transient oscillation compared to the UR.

Figure 10 shows the force evolution of ACF and UR10e for a desired velocity of $v_d = 0.25 \text{ m s}^{-1}$ and desired forces of $F_d = 15 \text{ N}$ and $F_d = 35 \text{ N}$. The orientation changes are challenging for both ACF and UR force control, and this partly leads to a loss of contact with the work piece. This particularly happens for the UR force control and causes force peaks when contact is regained. The effect of the jump is recognizable at a time of approx. $t = 6 \text{ s}$, with measured forces near zero for both ACF and UR, followed by another force peak

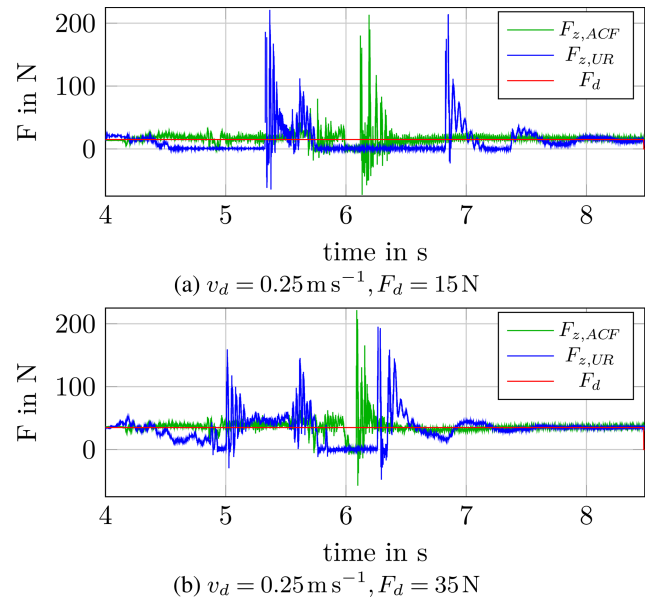


Figure 10. Force comparison of movement and standstill for the ramp profile.

with transient oscillation. However, the UR regains contact much later than the ACF. For the last 2 s of the trajectory, the robot should already stay constant at its end pose, but this is delayed due to the UR force control.

Table 1 summarizes the results for the ramp profile for the average of five test runs with desired velocity $v_d = 0.25 \text{ m s}^{-1}$. The ACF force control leads to much shorter settling times and also to lower force errors for both time domains of interest.

The corresponding UR motor currents for the whole path (first contact, movement, and standstill) for a desired force of $F_d = 15 \text{ N}$ are shown in Appendix A in Fig. A1. Oscillations due to UR force control are also visible in the measured currents.

7.2 Direct sensor contact

This test with a movement directly onto the force/torque sensor that checks the performance of the UR/ACF force control when the desired contact is 100 N . Considering the desired velocities of $v_d = 0.10 \text{ m s}^{-1}$ and $v_d = 0.25 \text{ m s}^{-1}$, the force evolution of Fig. 11 shows a very stable control behaviour of the ACF. This implies a significant advantage of the ACF-K 109/04 over the UR10e. Closely looking at the beginning of Fig. 11, it should be noted that the impact time varies due to the difference between UR position and force control. However, for the assessment the force evolution is synchronized to have the same contact time at $t = 0$.

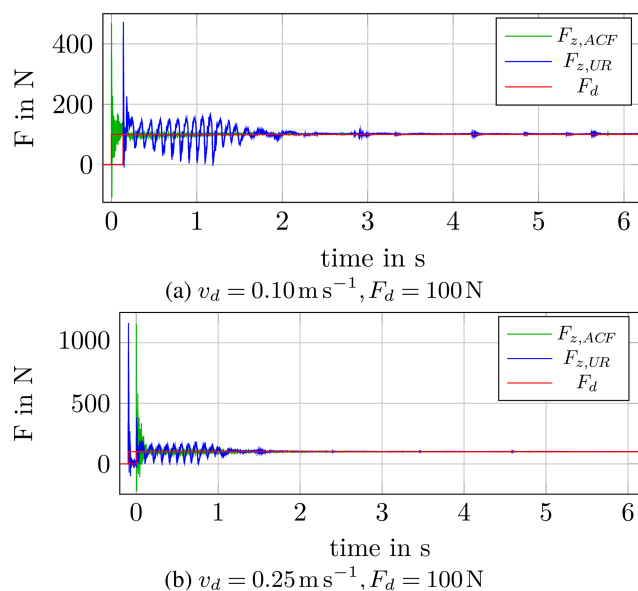
As shown in Table 2, using the average of five test runs, the stable control behaviour of the ACF, even for such a high force, leads to short settling times, especially compared to the UR. This results in much smaller absolute mean er-

Table 1. Assessment of ACF and UR force control, with the ramp profile ($v_d = 0.25 \text{ m s}^{-1}$). Bold font refers to $F_{z,ACF}$ and italic font to $F_{z,UR}$ data.

(a) First contact and standstill ($0 \text{ s} \leq t \leq t_c$)						
F_d in N	t_{ramp} in s	Gain scaling	t_{set} in s	$\text{Max} \Delta F_c $ in N	$\text{Mean} \Delta F_c $ in N	$\sigma \Delta F_c $ in N
15	0	<i>ACF</i>	0.22	279.70	3.27	13.71
	UR	1	1.00	362.80	10.68	25.63
35	0	<i>ACF</i>	0.29	291.70	3.23	15.03
	UR	1	0.57	340.58	8.80	25.04
(b) Movement and standstill ($t_m \leq t \leq t_e$)						
F_d in N	t_{ramp} in s	Gain scaling		$\text{Max} \Delta F_p $ in N	$\text{Mean} \Delta F_p $ in N	$\sigma \Delta F_p $ in N
15	0	<i>ACF</i>		410.93	5.73	14.73
	UR	1		381.76	14.14	24.03
35	0	<i>ACF</i>		216.46	5.33	10.38
	UR	1		431.50	14.75	24.47

Table 2. Assessment of ACF and UR force control, with the direct sensor contact ($F_d = 100 \text{ N}$).

v_d in m s^{-1}	t_{ramp} in s	Gain scaling	t_{set} in s	$\text{Max} \Delta F_c $ in N	$\text{Mean} \Delta F_c $ in N	$\sigma \Delta F_c $ in N
0.10	0	<i>ACF</i>	0.34	329.56	2.12	9.06
	UR	1		331.69	10.61	16.13
0.25	0	<i>ACF</i>	0.50	994.39	4.31	23.73
	UR	1	2.10	1067.18	12.52	31.74

**Figure 11.** Force comparison for the direct sensor contact.

rors $\text{Mean}|\Delta F_p|$ and standard deviations $\sigma|\Delta F_p|$ as well. For $v_d = 0.10 \text{ m s}^{-1}$, the UR force error exceeds the defined error band of $\pm 10 \text{ N}$, and so the oscillation time is impossible to evaluate. The force oscillations due to UR force control are also visible in the measured motor currents of Fig. B1.

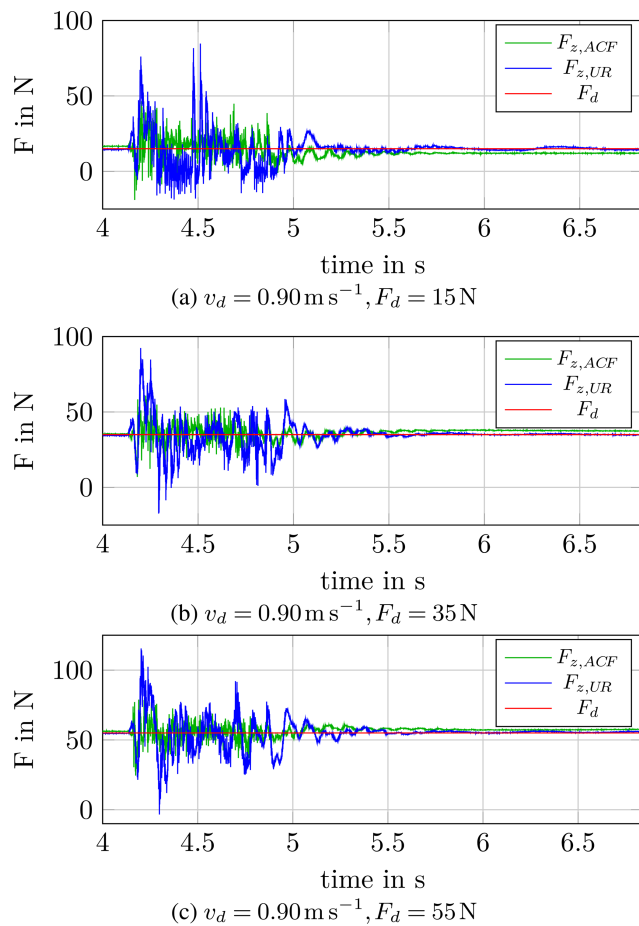
7.3 Straight profile

Figure 12 visualizes the forces of the straight profile for a desired TCP velocity of $v_d = 0.90 \text{ m s}^{-1}$ and the desired forces $F_d = 15 \text{ N}$, $F_d = 35 \text{ N}$ and $F_d = 55 \text{ N}$. The required horizontal movement for the straight profile simplifies the force control, but the ACF force control is superior. However, during the 2 s long standstill after the movement, the UR force control seems to lead to a marginally lower force offset.

Table 3 summarizes the results of the straight profile, again using the average of five test runs. The ACF achieves better results for the horizontal movement. In particular, the low absolute mean error $\text{Mean}|\Delta F_p|$ and corresponding standard deviation $\sigma|\Delta F_p|$ reveal the better performance for such high TCP velocity.

Table 3. Assessment of ACF and UR force control of movement and standstill, with the straight profile ($v_d = 0.90 \text{ m s}^{-1}$, $t_m \leq t \leq t_e$).

F_d in N	t_{ramp} in N	Gain scaling	Max $ \Delta F_p $ in N	Mean $ \Delta F_p $ in N	$\sigma \Delta F_p $ in N
15	0	ACF	58.17	3.97	4.22
	UR	1	70.11	4.61	7.94
35	0	ACF	29.12	3.02	2.87
	UR	1	58.72	4.07	7.12
55	0	ACF	32.19	2.70	2.78
	UR	1	62.26	4.62	8.00

**Figure 12.** Force comparison of movement and standstill for the straight profile.

For completeness, Fig. C1 shows the corresponding UR motor currents for the whole path for a desired force of $F_d = 55 \text{ N}$.

8 Conclusions

We proposed realistic test scenarios for the assessment of force control and experimentally evaluated the force control

of Universal Robots UR10e and FerRobotics ACF-K 109/04. The results confirm that the UR is well suited to simple, straight line motions with low speed, as it is the intended application for such a collaborative robot. In summary, the ACF force control works well for all tested velocities and forces and guarantees a short transient oscillation. It also shows superior force control behaviour for fast orientation changes. In contrast, the force control of UR10e is suitable to only a limited extent for such fast orientation changes because it temporarily loses contact with the work piece, especially for lower forces. However, the UR force control performance is appropriate for simple, straight line movements and lower velocities. As shown for the test cases, the UR force control performance decreases with increasing TCP velocity. In combination with high forces, and considering the tested parameters, the UR force control even exhibits stability problems. Yet, the UR10e is designed as a collaborative robot (cobot) and not as robot for surface finishing.

The proposed test scenarios for force control evaluation are applicable to general systems. So these test scenarios could serve as a standard force control test, similar to the ISO 9283 test for positioning accuracy evaluation. Future work, involving tests with other robots using different force control implementations or other force compliance devices, is required for a more generalized force control performance benchmarking.

Appendix A: Results for the ramp profile

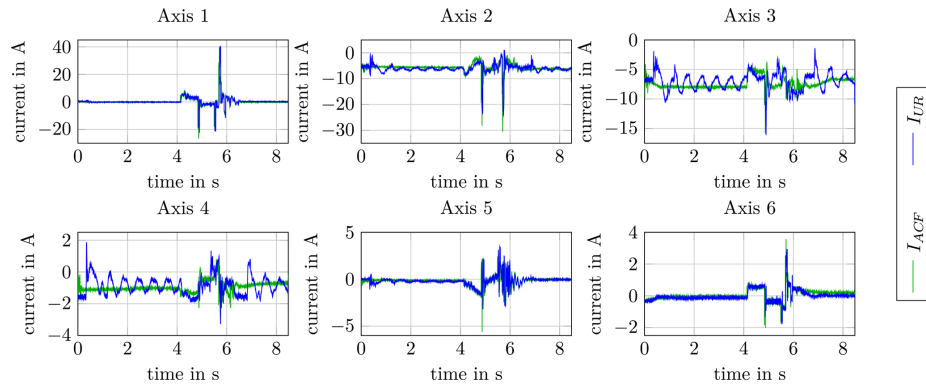


Figure A1. Motor currents of the UR drives for the ramp profile ($v_d = 0.25 \text{ m s}^{-1}$, $F_d = 15 \text{ N}$).

Appendix B: Results for the direct sensor contact

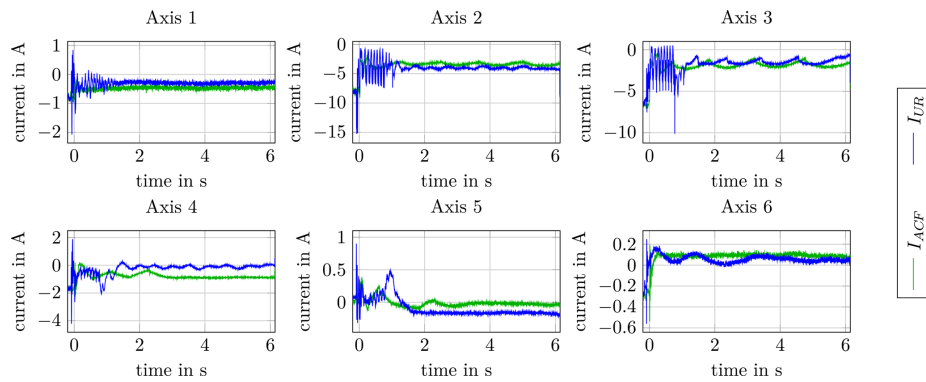


Figure B1. Motor currents of the UR drives for the direct sensor contact ($v_d = 0.25 \text{ m s}^{-1}$, $F_d = 100 \text{ N}$).

Appendix C: Results for the straight profile

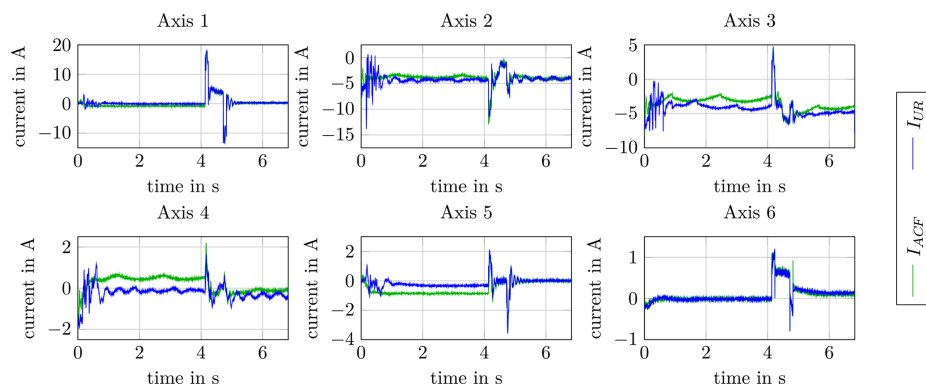


Figure C1. Motor currents of the UR drives for the straight profile ($v_d = 0.90 \text{ m s}^{-1}$, $F_d = 55 \text{ N}$).

Code and data availability. Universal Robots (UR script) programmes are provided on the GitHub repository of JKU Linz – Institute of Robotics (2022, https://github.com/JKU-Linz-Institute-of-Robotics/ur10e_force_control_comparison). All other data can be provided by the corresponding author upon request.

Video supplement. Videos from the test scenarios (ramp profile, direct sensor contact, and straight profile) can be provided by the corresponding author upon request.

Author contributions. All measurements and data analysis were performed by SG. SG wrote the draft, while AM and HG reviewed and edited the paper.

Competing interests. At least one of the (co-)authors is a member of the editorial board of *Mechanical Sciences*. The peer-review process was guided by an independent editor, and the authors also have no other competing interests to declare.

Disclaimer. Publisher's note: Copernicus Publications remains neutral with regard to jurisdictional claims in published maps and institutional affiliations.

Special issue statement. This article is part of the special issue “Advances in Service and Industrial Robotics – RAAD2021”. It is a result of the The 30th International Conference on Robotics in Alpe-Adria-Danube Region, RAAD 2021, Futuroscope-Poitiers, France, 21–23 June 2021.

Acknowledgements. This work has been supported by the LCM – K2 Center for Symbiotic Mechatronics within the framework of the Austrian COMET-K2 programme. For the assessment, the active contact flange ACF-K 109/04 was provided by FerRobotics Compliant Robot Technology GmbH.

Review statement. This paper was edited by Mohamed Amine Laribi and reviewed by Jozsef Tar and one anonymous referee.

References

ATI Industrial Automation: ATI Delta SI-660-60, https://www.ati-ia.com/products/ft/ft_models.aspx?id=Delta, last access: 6 December 2021a.

ATI Industrial Automation: Passive Compliant Force Control Device, https://www.ati-ia.com/products/deburr/ForceControl_Main.aspx, last access: 6 December 2021b.

B&R Industrial Automation GmbH: B&R X20 AI4632, <https://www.br-automation.com/en-gb/downloads/control-and-io-systems/x20-system-coated/analog-io-modules/analog-inputs/x20cai4632/datasheet-x20cai4632/>, last access: 11 February 2021a.

B&R Industrial Automation GmbH: B&R X20 CP3484, <https://www.br-automation.com/en-gb/downloads/control-and-io-systems/x20-system/cpus/x20cp3484/datasheet-x20cp3484/>, last access: 11 February 2021b.

Bremer, H.: Elastic Multibody Dynamics – A Direct Ritz Approach, Springer Netherlands, <https://doi.org/10.1007/978-1-4020-8680-9>, 2008.

FerRobotics Compliant Robot Technology GmbH: Active Contact Flange, <https://www.ferrobotics.com/en/services/products/active-contact-flange/>, last access: 6 December 2021a.

FerRobotics Compliant Robot Technology GmbH: Active Contact Flange Kit, <https://www.ferrobotics.com/en/services/products/active-contact-flange-kit/>, last access: 6 December 2021b.

FerRobotics Compliant Robot Technology GmbH: Active Contact Flange – User Manual, 2021c.

Fritsch, F. N. and Carlson, R. E.: Monotone Piecewise Cubic Interpolation, *SIAM J. Numer. Anal.*, 17, 238–246, 1980.

Iglesias, I., Sebastián, M., and Ares, J.: Overview of the state of robotic machining: Current situation and future potential, *Procedia Engineer.*, 132, 911–917, 2015.

JKU Linz – Institute of Robotics: UR10e Force Control Comparison, GitHub [code, data set] https://github.com/JKU-Linz-Institute-of-Robotics/ur10e_force_control_comparison, last access: 13 April 2022 (also available at Zenodo: <https://doi.org/10.5281/zenodo.6457906>).

PushCorp Inc.: Robotic Force Compliance Devices, <https://pushcorp.com/productcat/robotic-force-compliance-devices/>, last access: 6 December 2021.

Robotiq: Sanding Kit, <https://robotiq.com/products/sanding-kit>, last access: 6 December 2021.

Siciliano, B. and Khatib, O.: Springer Handbook of Robotics, Springer, 2nd Edn., 2016.

Siciliano, B. and Villani, L.: Robot Force Control, Springer Science & Business Media, 1999.

Universal Robots A/S: Universal Robot UR10e, <https://www.universal-robots.com/products/ur10-robot/>, last access: 6 December 2021.

Winkler, A. and Suchý, J.: Force Controlled Contour Following on Unknown Objects with an Industrial Robot, in: IEEE International Symposium on Robotic and Sensors Environments (ROSE), IEEE, 208–213, <https://doi.org/10.1109/ROSE.2013.6698444>, 2013.